

# Cloud response and feedback processes in stratiform mixed-phase clouds perturbed by ship exhaust

**Journal Article****Author(s):**

Possner, Anna; Ekman, Annica M.L.; Lohmann, Ulrike

**Publication date:**

2017-02-28

**Permanent link:**

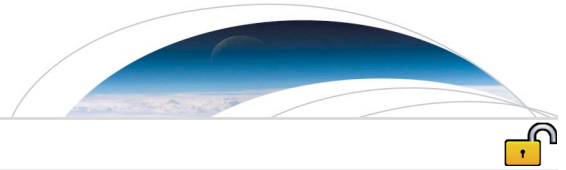
<https://doi.org/10.3929/ethz-b-000129188>

**Rights / license:**

[Creative Commons Attribution-NonCommercial-NoDerivatives 4.0 International](#)

**Originally published in:**


Geophysical Research Letters 44(4), <https://doi.org/10.1002/2016GL071358>



## RESEARCH LETTER

10.1002/2016GL071358

# Cloud response and feedback processes in stratiform mixed-phase clouds perturbed by ship exhaust

 Anna Possner<sup>1,2</sup> , Annica M. L. Ekman<sup>3</sup> , and Ulrike Lohmann<sup>1</sup> 

<sup>1</sup>Institute for Atmospheric and Climate Sciences, ETH Zurich, Zurich, Switzerland, <sup>2</sup>Department of Global Ecology, Carnegie Institution for Science, Stanford, California, USA, <sup>3</sup>Department of Meteorology and Bolin Centre for Climate Research, Stockholm University, Stockholm, Sweden

## Key Points:

- Increases in cloud top radiative cooling lead to increased immersion freezing rates near cloud top
- Feedback mechanisms involving the ice phase reduce, if not suppress, changes to the cloud liquid water path triggered by ship exhaust
- Changes in cloud condensation nuclei concentrations of  $100 \text{ cm}^{-3}$  were sufficient to shift the cloud state beyond its background variability

## Supporting Information:

- Supporting Information S1
- Figure S1
- Figure S2
- Figure S3

## Correspondence to:

A. Possner,  
apossner@carnegiescience.edu

## Citation:

Possner, A., A. M. L. Ekman, and U. Lohmann (2017), Cloud response and feedback processes in stratiform mixed-phase clouds perturbed by ship exhaust, *Geophys. Res. Lett.*, *44*, 1964–1972, doi:10.1002/2016GL071358.

Received 27 SEP 2016

Accepted 26 JAN 2017

Accepted article online 30 JAN 2017

Published online 18 FEB 2017

©2017. The Authors.

This is an open access article under the terms of the Creative Commons Attribution-NonCommercial-NoDerivs License, which permits use and distribution in any medium, provided the original work is properly cited, the use is non-commercial and no modifications or adaptations are made.

**Abstract** Stratiform mixed-phase clouds (MPCs), which contain both supercooled liquid and ice, play a key role in the energy balance of the Arctic and are a major contributor to surface precipitation. As Arctic shipping is projected to increase with climate change, these clouds may frequently be exposed to local aerosol perturbations of up to  $15,000 \text{ cm}^{-3}$ . Yet little consensus exists within the community regarding the key feedback mechanisms induced in MPCs perturbed by ship exhaust, or aerosol in general. Here we show that many known processes identified in the warm-phase stratocumulus regime can be extrapolated to the MPC regime. However, their effect may be compensated, or even undermined, by the following two most relevant processes unique to the MPC regime: (i) increased cloud glaciation via immersion freezing due to cloud condensation nuclei (CCN) induced cloud top radiative cooling and (ii) the continued cycling of ice nucleating particles (INPs) through the cloud and subcloud layer.

## 1. Introduction

The Arctic is warming due to increased anthropogenic greenhouse gas emissions, and it is doing so more rapidly than the rest of the globe. The International Panel on Climate Change estimates that the Arctic may warm by up to 8.3 K by the end of the century under the “business-as-usual” scenario, which is almost twice the projected mean global warming of  $3.7 \pm 1.1$  K by the end of the century [Collins *et al.*, 2013]. Concurrent with this regionally amplified warming, Arctic sea ice is melting rapidly. As the sea ice retreats, previously irretrievable natural resources become accessible and long-distance trade routes, such as the Northern Sea Route, become passable for 3 to 6 months of the year [Khon *et al.*, 2010]. As a result, the inner-Arctic shipping due to natural resource retrieval, transportation of goods and tourism, and trans-Arctic shipping are all projected to increase during the 21st century.

However, ship emissions themselves are not expected to increase linearly with rising shipping activity due to tighter emission regulations placed on  $\text{SO}_x$  and  $\text{NO}_x$  emissions [International Maritime Organization, 2008], which have been shown to lead to a drastic reduction of particle number and particulate mass emissions [Anderson *et al.*, 2015]. Nonetheless, ships are still expected to exert large local perturbations in aerosol particle concentration on the order of  $10^5 \text{ cm}^{-3}$  to an otherwise clean background where particle concentrations can be up to 3 to 4 orders of magnitude lower.

Many of the emitted particles are coated with a mixture of sulfate and nitrate, which have a strong affinity to take up water (hygroscopicity) or secondary organics, which are slightly hygroscopic [Verutbankul *et al.*, 2006] and may therefore act as a cloud condensation nuclei (CCN). As the exhaust plume enters the cloud, the cloud droplet number concentration may consequently increase locally. In warm clouds with constant liquid water content, this will inherently lead to smaller cloud droplets and induce local cloud brightening [Twomey, 1977]. In pure liquid stratocumulus clouds, such an influx of particles has been shown to also alter the cloud macrophysical state [Berner *et al.*, 2015] and to affect cloud lifetime [Ackerman *et al.*, 2004]. In rare cases, localized ship perturbations lead to streak-like structures of local cloud brightening—so-called ship tracks—which may span up to hundreds of kilometers in length but do not exert a climate-relevant radiative effect [Schreier *et al.*, 2007].

In the current Arctic climate, the oceans are cloud covered at least 60% of the time and most of these clouds (over 70%) are low-lying boundary layer clouds [Liu *et al.*, 2012]. During the autumn season, when the sea ice

extent reaches its minimum, Arctic cloud cover even exceeds 90%. Many of the boundary layer clouds will be mixed-phase clouds (MPCs) containing a mixture of supercooled cloud droplets and ice crystals. Arctic MPCs have captured the attention of many researchers in the past decades, due to their vast horizontal extent, significant radiative effect, and their longevity (lifetime of days to weeks) despite their microphysically unstable state [Morrison *et al.*, 2012].

As opposed to their liquid counterparts, many more microphysical pathways in which a potential aerosol perturbation may impact the cloud state exist in MPCs. At the relatively warm temperatures ( $T > 248$  K) found in Arctic MPCs, ice is predominantly formed by immersion freezing [Morrison *et al.*, 2012]. Hence, supercooled liquid droplets containing one or more ice-nucleating particles (INPs), will freeze at a given temperature constrained by the aerosol species acting as INPs at the highest temperature. Once ice is formed the crystals may sediment into regions subsaturated with respect to water, where they grow at the expense of the surrounding supercooled liquid due to their lower saturation vapor pressure [Wegener, 1911; Bergeron, 1935; Findeisen, 1938]. Thereby, the ice crystals deplete their own nucleation source before they exit the cloud, which will limit the formation of new ice crystals. In this manner an equilibrium between the two phases can be established and a MPC maintained.

The possible effect of ship emissions on this delicate microphysical balance remains highly uncertain. Christensen *et al.* [2014] concluded from satellite retrievals of MPCs obtained north of 40°N that ice water content and surface precipitation were increased by ship exhaust. Furthermore, they argued that the increase in ice could be caused by additional INP emissions from the ship besides the far more numerous CCN emissions.

In this study we use large eddy simulations to explore how many of the known feedback mechanisms detected in ship-perturbed warm-phase stratocumulus extend to the MPC regime and which additional feedback mechanisms occur in MPCs that may alter the cloud response.

## 2. Model Description and Setup

Large eddy simulations (LES) are performed with the Consortium for Small-scale Modeling (COSMO) model in its configuration for idealized LES experiments. A more detailed model description is provided in the supporting information [Bott, 1989; Foerstner and Doms, 2004; Lack *et al.*, 2009; Louis, 1979; Mironov and Raschendorfer, 2001; Nenes and Seinfeld, 2003; Possner *et al.*, 2015; Ritter and Geleyn, 1992; Wicker and Skamarock, 2002]. The simulations were performed for a single-layer MP stratus case observed on October 9th and 10th, 2004 during the MP Arctic Cloud Experiment, M-PACE [Verlinde *et al.*, 2007]. The simulations are initialized and dynamically forced following the LES intercomparison protocol by Klein *et al.* [2009] with a fixed horizontal resolution of 50 m and a time step of 2 s. The vertical resolution is variable and specified with 10 m within the cloud layer and at most 160 m within the subcloud layer. The cloud microphysical tendencies are parameterized following the Seifert and Beheng [2006] two-moment scheme. Background CCN are diagnosed every time step following Köhler theory for a fixed aerosol size distribution of ammonium bisulfate. In order to study the effects of instantaneous cloud seeding by ship exhaust, prognostic CCN concentrations of ship exhaust are implemented for ship emissions (Table S1 in the supporting information). Prognostic INPs are treated as in Solomon *et al.* [2015] in order to study feedback processes involving variable  $N_i$ . This scheme parameterizes immersion freezing following the DeMott *et al.* [2015] temperature dependence and captures the depletion and replenishing of INPs (see supporting information for further reference).

Mean INP concentrations for nucleation in the deposition, condensation, or immersion mode of  $0.16 \text{ L}^{-1}$  for particles smaller than  $2 \mu\text{m}$  were measured on board the Citation aircraft [Prenni *et al.*, 2007] during the M-PACE campaign, while local concentrations as high as  $12 \text{ L}^{-1}$  (at 259 K) were measured. However, the mass-weighted median ice crystal number concentration ( $N_i$ ) measured on board the same aircraft [McFarquhar *et al.*, 2007] was  $\sim 2 \text{ L}^{-1}$  and exceeded the mean INP concentration by an order of magnitude. Some of this discrepancy may have been a measurement artifact caused by the shattering of ice crystals upon impaction with the inlet tips of the aircraft, which artificially enhanced ice crystal number concentrations [Field *et al.*, 2006]. For this reason only ice crystals larger than  $53 \mu\text{m}$  were considered in the analysis by McFarquhar *et al.* [2007], which at least partially accounts for this artifact. Several secondary ice processes, which may close the gap between INPs and  $N_i$ , have been suggested. Evaporation freezing and the release of potential INPs during the evaporation of cloud or rain drops were shown to be potentially dominant processes in enhancing  $N_i$  in LES simulations [Fridlind *et al.*, 2007]. However, secondary ice processes in stratiform MPCs remain highly

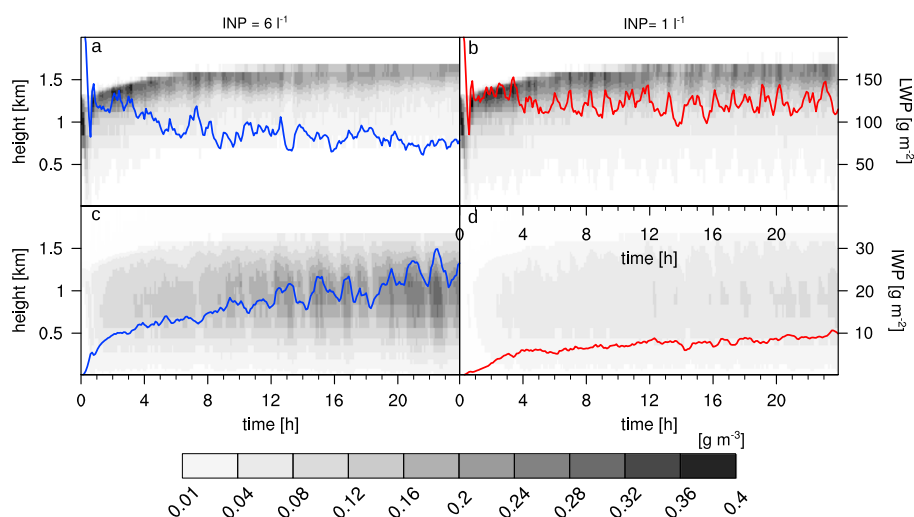


**Figure 1.** (a, b) Liquid water content ( $\text{g m}^{-3}$ ) and (c, d) ice water content scaled by factor 10 to match the liquid water content contour intervals for the two reference simulations INPini6 and INPini1 (grey shading). The evolution of the liquid water path ( $\text{g m}^{-2}$ ) and ice water path ( $\text{g m}^{-2}$ ) is shown for INPini6 (left column, blue lines) and INPini1 (right column, red lines).

uncertain and unconstrained by observations. For this reason, secondary ice processes, other than allowing INPs to freeze multiple times, are omitted in the present study and two different background state simulations (shown in Figure 1) were considered instead. For one simulation, an initial INP concentration of  $6 \text{ L}^{-1}$  (INPini6) was chosen in order to match observed ice crystal number concentrations. In a second simulation, a more realistic initial INP concentration of  $1 \text{ L}^{-1}$  (INPini1) was prescribed, but  $N_i$  was underestimated (by an order of magnitude) and mostly liquid-phase surface precipitation was simulated, as opposed to the observed record of ice-phase precipitation. However, the simulated ice water path remained within the range of uncertainty of the observations.

For simulations representing cloud perturbations by ship exhaust, the physically plausible space of aerosol number perturbations relevant for CCN activation ( $\text{CCN}_{\text{ship}} = 0\text{--}15,000 \text{ cm}^{-3}$ ) and INP perturbations ( $\text{INP}_{\text{ship}} = 0\text{--}5 \text{ L}^{-1}$ ) was simulated. The covered range of  $\text{CCN}_{\text{ship}}$  was split into eight equally, logarithmically spaced bins, while three linearly spaced bins were used for the  $\text{INP}_{\text{ship}}$  emissions. The  $\text{INP}_{\text{ship}} > 0 \text{ L}^{-1}$  simulations were performed for every second  $\text{CCN}_{\text{ship}}$  bin for run time efficiency, resulting in a total of 46 performed simulations. The ship exhaust perturbation is released instantaneously after 10 h of simulation as a homogeneous increase in aerosol concentrations over the whole domain.

### 3. Results

The two unperturbed reference simulations, INPini1 and INPini6, which do not contain any ship emissions, show a high degree of agreement with the M-PACE campaign observations and other LES simulations [Klein *et al.*, 2009]: The initially rapid boundary layer growth slows after 4 h of simulation until a cloud top height of 1.5 km is reached after  $\sim 10$  h (Figure 1). During this initial growth period, the subcloud layer near cloud base stabilizes, as is seen in the positive vertical gradient of the ice-liquid potential temperature and negative vertical gradient in the total water content in this region (Figure 2). The level of stability below cloud base is maintained throughout the remainder of the simulation and can be attributed to the release of latent heat during the depositional growth of snow and ice crystals near cloud base ( $\partial T / \partial t \sim 0.4 \text{ K h}^{-1}$ ).

The simulated ice water content and ice water path (IWP) are within the observed range measured on board the Citation aircraft during the M-PACE campaign [McFarquhar *et al.*, 2007] and ground-based radar/lidar measurements obtained at Oliktok point, Alaska [Shupe *et al.*, 2006; Turner *et al.*, 2007]. The liquid water content and liquid water path (LWP) are underestimated in the INPini6 simulation, where ice crystal number concentrations in agreement with observations ( $\bar{N}_i \sim 1.2 \text{ L}^{-1}$ ) are simulated. On the other hand, the liquid water

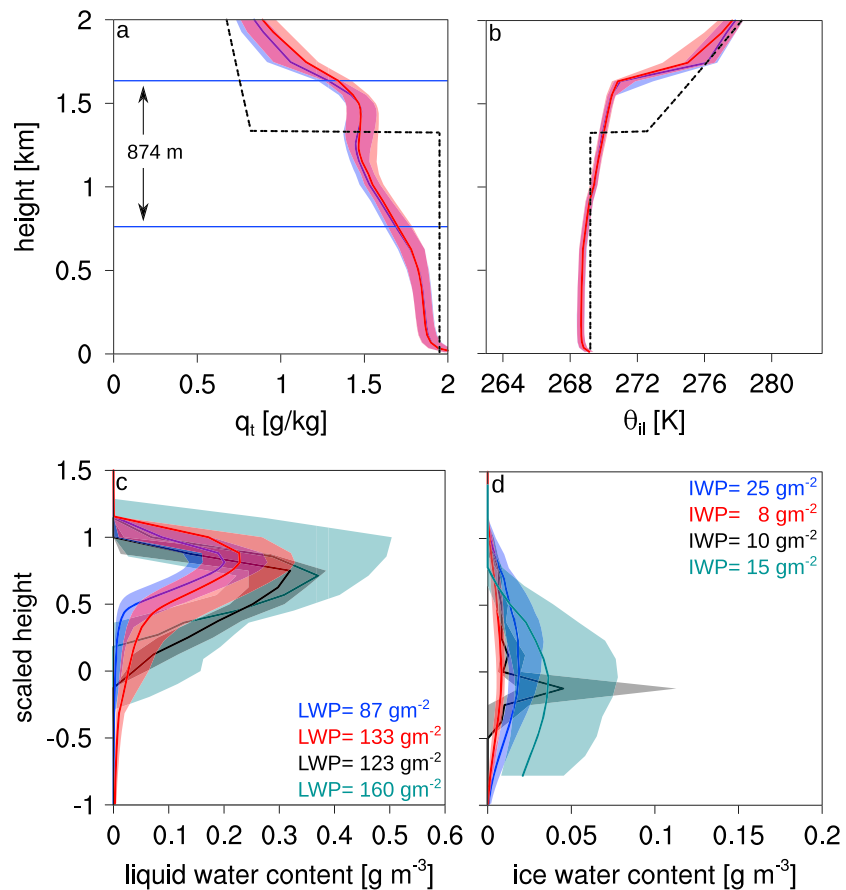


**Figure 2.** Median values and interquartile ranges obtained between 10 and 24 h of the simulated period for the INPini6 reference simulation (blue) and the INPini1 reference simulation (red) together with observations (black and cyan, only Figures 2c and 2d). (a) Total water content  $q_t = q_v + q_c + q_i$ , where  $q_v$  is the water vapor content,  $q_c$  the cloud water content, and  $q_i$  the ice water content. Blue horizontal lines in Figure 2a denote the mean cloud top and cloud base. (b) Ice-liquid-water potential temperature profile. The dashed profiles depict the initial profiles obtained from the Barrow sounding. (c) Liquid water content and (d) ice water content in comparison with aircraft observations [McFarquhar et al., 2007] in black and radar/lidar measurements [Shupe et al., 2006; Turner et al., 2007] and in cyan obtained during the M-PACE campaign. Integrated quantities, liquid water path (LWP) in Figure 2c and ice water path (IWP) in Figure 2d are given in the lower right and upper right corners, respectively. Height in Figures 2c and 2d is scaled with respect to the cloud base and cloud top, where 1 denotes the cloud top, 0 the cloud base, and -1 the surface.

content is captured well in the INPini1 simulation, where, instead,  $N_i$  is underestimated by an order of magnitude. However, it should be noted that all simulations fall within the model spread obtained during the Klein et al. [2009] intercomparison study of this case (LWP: 20.2–222  $\text{g m}^{-2}$ , IWP: 0.03–34  $\text{g m}^{-2}$ ).

The total amount of surface precipitation is not substantially affected by the partitioning of the total water content into liquid and ice. However, most of the precipitation in INPini1 falls as rain, while almost all precipitation falls as snow in the INPini6 simulation, which is in agreement with surface precipitation measurements. In the latter simulation rain still forms but evaporates in the subcloud layer.

The ship emission impacts induced in both reference states of the simulated clean cloud are discussed in the following sections for emission perturbations consisting purely of CCN (section 3.1) and consisting of CCN and INP emissions (section 3.2).

### 3.1. Effects of CCN From Ship Emissions

The cloud response to ship exhaust perturbations increasing the CCN and cloud droplet number concentration ( $N_p$ ) is found to largely depend on the background state of the cloud (Figure 3). While traditional feedback processes found in pure liquid marine stratocumulus are also found in MPCs, additional microphysical feedback processes involving the ice phase are triggered, which alter the cloud evolution.

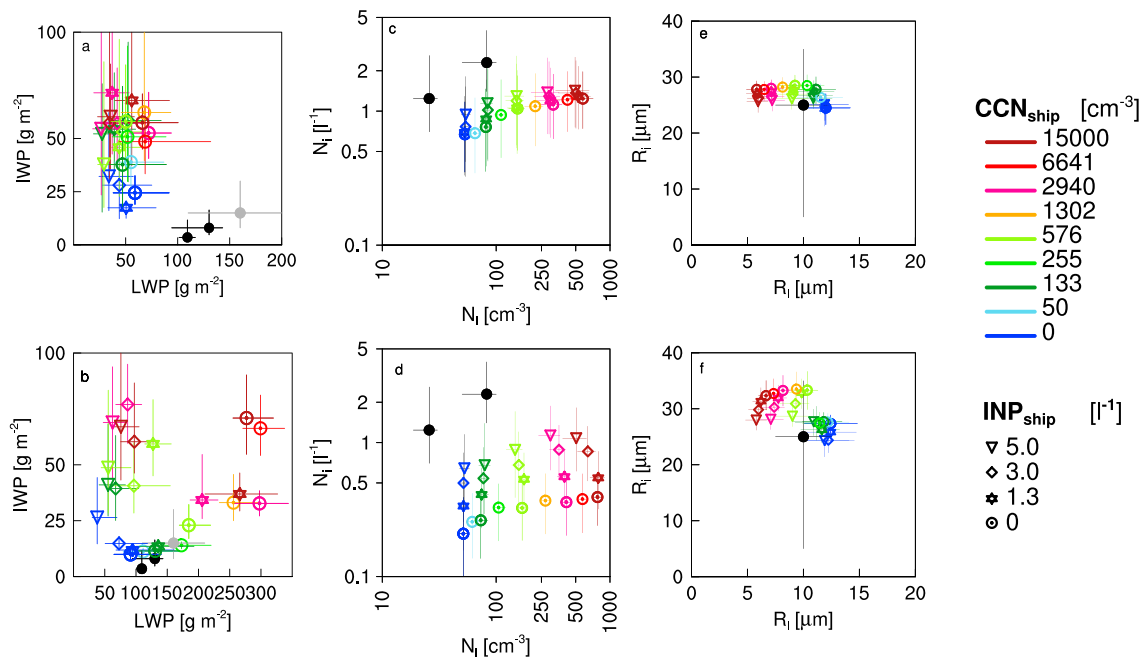


**Figure 3.** Median response obtained between 10 and 24 h of simulation in (a) LWP and (b) IWP, (c) ice crystal and (d) cloud droplet number concentration ( $N_i$  and  $N_j$ ), and (e) effective ice crystal and (f) cloud droplet radius ( $R_i$  and  $R_j$ ) to  $CCN_{ship}$  and  $INP_{ship}$  perturbations in INPini6 simulations (Figures 3a, 3c, and 3e), and INPini1 simulations (Figures 3b, 3d, and 3f). The interquartile range is denoted by lines. Variability in aircraft observations for 9 and 10 October 2004 [McFarquhar et al., 2007] is plotted in black and radar/lidar observations [Shupe et al., 2006; Turner et al., 2007] in grey.

As the MPC is seeded with  $CCN$ ,  $N_i$  increases and the number weighted droplet radius ( $R_i$ ) decreases almost instantaneously (Figure 3). This effect is commonly known as the *Twomey* [1977] effect and is regularly observed in warm-phase stratocumulus ship tracks [e.g., Hobbs et al., 2000; Christensen and Stephens, 2011]. Consequently, the formation of rain is reduced within the seeded cloud. In simulations where the surface precipitation almost entirely consists of rain (INPini1 simulations), the surface precipitation is reduced by more than 50% (Table S2) and the LWP increases from 91 g m<sup>-2</sup> to 230 g m<sup>-2</sup> (Figure 3) in simulations where  $CCN_{ship}$  perturbations exceed 1000 cm<sup>-3</sup>.

Due to the elevated cloud water content in the seeded clouds, the 75th percentile of the radiative cooling near the cloud top increases in magnitude from  $-0.6 \text{ K h}^{-1}$  to  $-2.3 \text{ K h}^{-1}$  (see Figure S1). In seeded warm-phase stratocumulus, the destabilization due to increased cloud top radiative cooling could enhance turbulent mixing generated near the cloud top, thereby increasing the cloud top entrainment [Ackerman et al., 2004]. Whether or not this feedback process would further enhance, or even revert the LWP response due to precipitation suppression in ship tracks, was found to depend on the free troposphere moisture content [Chen et al., 2015]. However, in the MPC regime, additional mechanisms are triggered, which stabilizes the cloud top and to some degree suppress the enhancement of entrainment.

In regions of increased cloud top cooling, we also detect increased levels of freezing in our simulations. Most ice crystals form by immersion freezing near the cloud top, where the coldest temperatures are reached just below the inversion. The increase in cloud top radiative cooling triggers the heterogeneous nucleation on additional INPs, which previously remained inactive as the temperature was too high in the clean cloud. In this manner  $N_i$  is increased from  $0.6 \text{ L}^{-1}$  ( $0.2 \text{ L}^{-1}$ ) to  $1.3 \text{ L}^{-1}$  ( $0.4 \text{ L}^{-1}$ ) in simulations with high (low) background INPs. Hence, the increase in cloud top cooling enables the formation of additional ice crystals in simulations solely perturbed by  $CCN$  emissions.

Changes in ice crystal radius ( $R_i$ ) between the polluted and clean simulations are small ( $\frac{\Delta R_i}{R_i} < 18\%$ ). Therefore, as more ice crystals freeze, more latent heat is released into the environment during liquid-ice (freezing) and vapor-ice (depositional growth) phase transitions (see Figure S2). Thereby, the additional freezing stabilizes the seeded cloud by partially compensating the generated instability due to the increased radiative cooling.

In the INPini6 simulations, where the change in  $N_i$  is on the order of  $1 \text{ L}^{-1}$  (locally), the increased release of latent heat balances the enhanced cloud top radiative cooling, such that the turbulent mixing and entrainment rate (not shown) remain invariant. Furthermore, once the ice crystals sediment below cloud base, they are sublimated and the INPs are released and mixed up into the cloud where they once again may initiate freezing. In this manner the increased levels of  $N_i$  are maintained from the point of instantaneous seeding for the remainder of the simulation (14 h).

In the INPini1 simulations, where the absolute change in  $N_i$  is considerably smaller ( $\mathcal{O}(0.2) \text{ L}^{-1}$ ), the latent heat released is insufficient to balance the radiative cooling enhancement. Therefore, the turbulent mixing near cloud top is increased and the seeded cloud deepens ( $\mathcal{O}(100) \text{ m}$ ) due to entrainment (Figure S1).

### 3.2. Response to Additional INP Emissions From Ships

The extent to which INP emissions ( $\text{INP}_{\text{ship}} = 0\text{--}5 \text{ L}^{-1}$ ) alter the cloud response in our simulations largely depends on the induced change in  $N_i$  which is governed by the following: (i) the increase in cloud top radiative cooling and (ii) the concentration of potential INPs which cause heterogeneous nucleation at temperatures colder than the cloud-top temperature of the clean cloud.

In the INPini6 simulations the  $\text{INP}_{\text{ship}}$  perturbations have little impact on the cloud evolution due to compensating effects [Glassmeier and Lohmann, 2016]. The emission of new INPs merely enhances the IWP response to  $\text{CCN}_{\text{ship}}$  perturbations by 12% (Figure 3) and increases surface precipitation slightly (Table S2). An impact of  $\text{INP}_{\text{ship}}$  on  $N_i$  is only seen in INPini6 simulations at small  $\text{CCN}$  perturbations ( $\text{CCN}_{\text{ship}} < 200 \text{ cm}^{-3}$ ), where the increase in cloud top radiative cooling and therefore the temperature change near cloud top is small.

However, in the INPini1 simulations, adding  $\text{INP}_{\text{ship}}$  alongside  $\text{CCN}_{\text{ship}}$  emissions changes the cloud evolution notably (Figure 3). As  $\text{INP}_{\text{ship}}$  increases, the LWP response to the  $\text{CCN}_{\text{ship}}$  perturbation is increasingly suppressed and the ice content in the cloud is increased. Thus, similar feedback processes are seen in the INP seeded clouds in the INPini1 simulations as in the INPini6 simulations with  $\text{INP}_{\text{ship}} = 0 \text{ L}^{-1}$ .

## 4. Discussion

Our results show that many of the feedback mechanisms identified in ship-perturbed warm-phase stratocumulus, such as the Twomey [1977] effect, liquid precipitation suppression, and entrainment enhancement, may also be found in the MPC regime. However, their impact may be partially compensated or even diminished by additional feedback processes involving the ice phase. A conceptual summary of all involved processes is given in Figure 4.

The range of identified processes is largely consistent with insights obtained from global satellite retrievals of ship tracks in MPCs by Christensen *et al.* [2014]. However, additional processes were identified in our simulations, which play a crucial role in determining the cloud response. The most important feedback process is mediated by the cloud top radiative cooling. Increases in cloud top radiative cooling due to liquid precipitation suppression by  $\text{CCN}$  seeding is found to enhance the immersion freezing near the cloud top. It is important to note that our simulations show that the additional INP may stem from ships, but do not have to. Figures 3 and 4 show that additional INPs, which freeze via immersion freezing, could also stem from the background aerosol population by initiating heterogeneous nucleation at lower cloud-top temperatures. Therefore this study highlights the importance of the cloud-top radiative feedback not only for the cloud and boundary layer dynamics but also for the glaciation levels of the MPC, as had also been noted by Savre and Ekman [2015].

Christensen *et al.* [2014] found that on average the ice water content detected in ship tracks was increased by 19%, the surface precipitation was increased by 30%, and the total water path decreased by 15% compared to the background. While we also find increases in ice water content in our simulations, our results differ in sign in the precipitation and total water path response. This difference may be attributed to (i) the particularly strong surface fluxes during the cold air outbreak simulated here, which may compensate the increased drying by entrainment at the cloud top and (ii) the sublimation of ice crystals in the subcloud layer which buffers changes in surface precipitation.

Increases in surface precipitation are only found in simulations with the largest changes in  $\text{INP}_{\text{ship}}$ . In all other simulations the surface precipitation remained unchanged or was decreased in simulations containing few ice crystals ( $N_i < 0.6 \text{ L}^{-1}$ ). This is due to the efficient sublimation of ice crystals below cloud base.

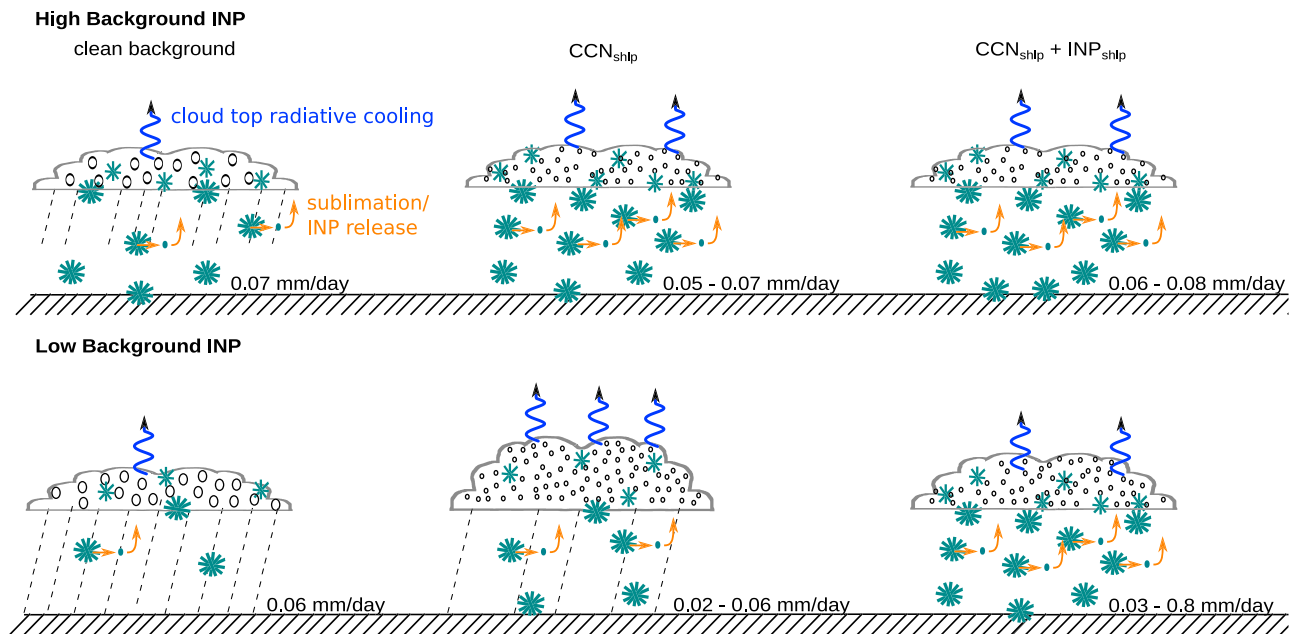


**Figure 4.** Conceptual schematic of ship emission impacts on Arctic stratiform MPCs. Cloud seeding with CCN reduces liquid precipitation and increases the cloud water content. Thereby, the cloud top radiative cooling is enhanced and the immersion freezing near the cloud top increased. In the high background INP (HBI) scenario,  $N_i$  increases and the LWP remains similar. In the low background INP (LBI) scenario, only few additional  $N_i$  are obtained by immersion freezing and additional turbulence and entrainment are generated due to cloud top cooling. Therefore, the cloud depth and LWP increase in the LBI scenario. Cloud seeding with INP in addition to CCN has little impact on the cloud response in the HBI scenario. However, in the LBI scenario adding INP alongside CCN elevates feedback processes involving the ice phase, which partially suppresses the LWP and boundary layer growth triggered by CCN emissions. Changes in  $N_i$  do not substantially impact surface precipitation, due to efficient subcloud sublimation during which INP are released and may reenter the cloud and trigger further heterogeneous nucleation events.

Furthermore, upon complete sublimation of crystals, INPs are released and in this manner may be cycled several times through the cloud before sedimenting to the surface. The process of INP recycling has previously been shown to be important for clouds observed during the M-PACE campaign [Verlinde *et al.*, 2007; Fan *et al.*, 2009] and other Arctic case studies [Solomon *et al.*, 2015]. Here we show that this process may also be highly relevant in determining the cloud response in aerosol-perturbed MPCs. In simulations where the sublimation of ice crystals was turned off, a much smaller response in the ice phase was simulated and the LWP began to increase (Figure S3).

Finally, the inclusion of ice phase processes strongly reduces the ship-induced change in the surface radiative forcing from that of a pure-liquid cloud. Reductions up to 200% in the net downward shortwave and longwave forcings (Table S3) are obtained as feedback processes through the ice phase increasingly dominate over the pure-liquid response. Hence, these simulations support the conclusion by Christensen *et al.* [2014] and Kravitz *et al.* [2014] that ship emissions are unlikely to exert a significant surface forcing offsetting Arctic warming.

### 5. Conclusions

This study provides a first in-depth numerical assessment of feedback mechanisms in MPCs induced by ship emissions, which are projected to increase significantly by the end of this century. We showed that many of the known feedback mechanisms observed in warm-phase stratocumulus perturbed by ship emissions are also found in the MPC regime. However, their effect may be fully compensated by feedback mechanisms triggered in the ice phase (Figure 4).

These feedback processes were identified in a set of 46 simulations which span a physically feasible range of CCN and INP perturbations. In particular, two feedback mechanisms were identified, which neither had been previously discussed in the literature nor had been addressed within this context (point 2). The key findings of this study are summarized as follows:

1. Cloud top radiative cooling triggered by CCN emissions and subsequent precipitation suppression enhanced the immersion freezing rate near cloud top. Thereby, the ice content of the cloud is increased



and the cloud layer is stabilized as changes in turbulent mixing near cloud top as well as entrainment rates are suppressed.

- The cycling of INP through the cloud and subcloud layer and subsequent freezing events induced by these INP near the cloud top were found to be important to sustain elevated ice crystal number and mass concentrations for a prolonged period in the perturbed cloud.
- Feedback processes within the ice phase reduce, if not inhibit, changes to the liquid water content of the cloud, which governs the cloud's radiative forcing and the boundary layer dynamics.
- Finally, these simulations showed that aerosol perturbations as low as  $100 \text{ cm}^{-3}$  were sufficient to shift the cloud state beyond its background variability. Therefore, this discussion may be relevant to not only ship exhaust perturbations but also other anthropogenic aerosol sources in the Arctic such as gas flaring and long-range transport of biomass burning [Hirdman et al., 2010].

#### Acknowledgments

This work was carried out at ETH Zurich in Switzerland and was supported by the Global Atmospheric Watch (GAW) program as well as the European Union funded project on Biogenic versus Anthropogenic emissions on Clouds and Climate (BACCHUS). All simulations were performed with the Consortium for Small-scale Modeling (COSMO) model adapted for large eddy simulations. All simulations were performed and are stored at the Swiss National Supercomputing Centre (SCS) and can be made accessible upon request. The radar/lidar observations were obtained from <ftp://ftp1.esrl.noaa.gov/psd3/arctic/barrow/shupeturner/microphysics/variablecoeff/> and the aircraft observations from <https://www.arm.gov/campaigns/nsa2004arcticlid>.

#### References

- Ackerman, A. S., M. P. Kirkpatrick, D. E. Stevens, and O. B. Toon (2004), The impact of humidity above stratiform clouds on indirect aerosol climate forcing, *Nature*, *432*, 1014–1017.
- Anderson, M., K. Salo, and E. Fridell (2015), Particle- and gaseous emissions from an LNG powered ship, *Environ. Sci. Technol.*, *49*(20), 12,568–12,575, doi:10.1021/acs.est.5b02678.
- Bergeron, T. (1935), On the physics of clouds and precipitation, in *Proces Verbaux de l'Association de Météorologie, 5th Assembly of the International Union of Geodesy and Geophysics*, edited by P. Dupont, pp. 156–178, Paris.
- Berner, A. H., C. S. Bretherton, and R. Wood (2015), Large eddy simulation of ship tracks in the collapsed marine boundary layer: A case study from the Monterey area ship track experiment, *Atmos. Chem. Phys.*, *15*, 5851–5871.
- Bott, A. (1989), A positive definite advection scheme obtained by nonlinear renormalization of the advective fluxes, *Mon. Weather Rev.*, *117*, 1006–1015.
- Chen, G., W.-C. Wang, and J.-P. Chen (2015), Aerosol-stratocumulus-radiation interactions over the southeast Pacific, *J. Atmos. Sci.*, *72*, 2612–2621.
- Christensen, M., and G. Stephens (2011), Microphysical and macrophysical responses of marine stratocumulus polluted by underlying ships: 2. Impacts of haze on precipitating clouds, *J. Geophys. Res.*, *116*, D11203, doi:10.1029/2010JD014638.
- Christensen, M. W., K. Suzuki, B. Zambri, and G. L. Stephens (2014), Ship track observations of a reduced shortwave aerosol indirect effect in mixed-phase clouds, *Geophys. Res. Lett.*, *41*, 6970–6977, doi:10.1002/2014GL061320.
- Collins, M., et al. (2013), Climate change: Projections, commitments and irreversibility, in *Climate Change 2013: The Physical Science Basis. Contribution of Working Group I to the Fifth Assessment Report of the Intergovernmental Panel on Climate Change*, edited by T. Stocker et al., pp. 571–658, Cambridge Univ. Press, Cambridge, U. K., and New York.
- DeMott, P. J., et al. (2015), Integrating laboratory and field data to quantify the immersion freezing ice nucleation activity of mineral dust particles, *Atmos. Chem. Phys.*, *15*, 393–409, doi:10.5194/acp-15-393-2015.
- Fan, J., M. Ovchinnikov, J. M. Comstock, S. A. McFarlane, and A. Khain (2009), Ice formation in Arctic mixed-phase clouds: Insights from a 3-D cloud-resolving model with size-resolved aerosol and cloud microphysics, *J. Geophys. Res.*, *114*, D04205, doi:10.1029/2008JD010782.
- Field, P. R., A. J. Heymsfield, and A. Bansemmer (2006), Shattering and particle inter-arrival times measured by optical array probes in ice clouds, *J. Atmos. Oceanic Technol.*, *23*, 1357–1371.
- Findeisen, W. (1938), Kolloid-meteorologische vorgänge bei niederschlagsbildung, *Meteorol. Z.*, *55*, 121–133.
- Foerstner, J., and G. Doms (2004), Runge-Kutta time integration and high-order spatial discretization of advection—A new dynamical core for the LMK, Model Development and Application, COSMO Newsl. No. 4. [Available at <http://www.cosmo-model.org/content/model/documentation/newsletters/newsLetter04/chp9-6.pdf>.]
- Fridlind, A. M., A. S. Ackerman, G. McFarquhar, G. Zhang, M. R. Poellot, P. J. DeMott, A. J. Prenni, and A. J. Heymsfield (2007), Ice properties of single-layer stratocumulus during the Mixed-Phase Arctic Cloud Experiment: 2. Model results, *J. Geophys. Res.*, *112*, D24202, doi:10.1029/2007/JD008646.
- Glassmeier, and F., U. Lohmann (2016), Constraining precipitation susceptibility of warm-, ice-, and mixed-phase clouds with microphysical equations, *J. Atmos. Sci.*, *73*, 5003–5023, doi:10.1175/JAS-D-16-0008.1.
- Hirdman, D., H. Sodemann, S. Eckhardt, J. F. Burkhart, A. Jefferson, T. Mefford, P. K. Quinn, S. Sharma, J. Ström, and A. Stohl (2010), Source identification of short-lived air pollutants in the Arctic using statistical analysis of measurement data and particle dispersion model output, *Atmos. Chem. Phys.*, *10*, 669–693, doi:10.5194/acp-10-669-2010.
- Hobbs, P. V., et al. (2000), Emissions from ships with respect to their effects on clouds, *J. Atmos. Sci.*, *57*, 2570–2590.
- International Maritime Organization (2008), MEPC 58/23/Add.1, Annex 14, RESOLUTION MEPC.177 adopted on 10 October 2008, Ammendments to the technical code on control of emissions of nitrogen oxides from marine diesel engines (NO<sub>x</sub> Technical Code 2008). International Maritime Organization - Marine Environment Protection Committee, London.
- Khon, V. C., I. I. Mokhov, A. Latif, V. A. Semenov, and W. Park (2010), Perspectives of Northern Sea Route and Northwest Passage in the twenty-first century, *Clim. Change*, *100*(3), 757–768, doi:10.1007/s10584-009-9683-2.
- Klein, S. A., et al. (2009), Intercomparison of model simulations of mixed-phase clouds observed during the ARM Mixed-Phase Arctic Cloud Experiment. I: Single-layer cloud, *Q. J. R. Meteorol. Soc.*, *135*, 979–1002, doi:10.1002/qf.416.
- Kravitz, B., H. Wang, P. Rasch, H. Morrison, and A. Solomon (2014), Process-model simulations of cloud albedo enhancement by aerosols in the Arctic, *Philos. Trans. R. Soc. A*, *372*, 20140052, doi:10.1098/rsta.2014.0052.
- Lack, D. A., et al. (2009), Particulate emissions from commercial shipping: Chemical, physical and optical properties, *J. Geophys. Res.*, *114*, D00F04, doi:10.1029/2008JD011300.
- Liu, Y., J. R. Key, S. A. Ackerman, G. G. Mace, and Q. Zhang (2012), Arctic cloud macrophysical characteristics from CloudSat and CALIPSO, *Remote Sens. Environ.*, *124*, 159–173.
- Louis, J.-F. (1979), A parametric model of vertical eddy fluxes in the atmosphere, *Boundary Layer Meteorol.*, *17*, 187–202.
- McFarquhar, G. M., G. Zhang, M. R. Poellot, G. L. Kok, R. McCoy, T. Tooman, A. Fridlind, and A. J. Heymsfield (2007), Ice properties of single-layer stratocumulus during the Mixed-Phase Arctic Cloud Experiment: 1. Observations, *J. Geophys. Res.*, *112*, D24201, doi:10.1029/2007JD008633.

- Mironov, D., and M. Raschendorfer, (2001), Evaluation of empirical parameters of the new LM surface-layer parameterization scheme, *Tech. Rep.*, German Weather Service, Offenbach, Germany. [Available at [www.cosmomodel.org](http://www.cosmomodel.org).]
- Morrison, H., G. de Boer, G. Feingold, J. Harrington, M. D. Shupe, and K. Sulia (2012), Resilience of persistent Arctic mixed-phase clouds, *Nat. Geosci.*, *5*, 11–17, doi:10.1038/ngeo1332.
- Nenes, A., and J. H. Seinfeld (2003), Parameterization of cloud droplet formation in global climate models, *J. Geophys. Res.*, *108*(D14), 4415, doi:10.1029/2002JD002911.
- Possner, A., E. Zubler, U. Lohmann, and C. Schär (2015), Real-case simulations of aerosol-cloud interactions in ship tracks over the Bay of Biscay, *Atmos. Chem. Phys.*, *15*, 2185–2201.
- Prenni, A. J., I. Y. Harrington, M. Tjernström, P. J. DeMott, A. Avramov, C. N. Long, S. M. Kreidenweis, P. Q. Olsson, and J. Verlinde (2007), Can ice-nucleating aerosols affect Arctic seasonal climate?, *Bull. Am. Meteorol. Soc.*, *88*, 541–550.
- Ritter, B., and J. F. Geleyn (1992), A comprehensive radiation scheme for numerical weather prediction models with potential applications in climate simulations, *Mon. Weather Rev.*, *120*, 303–325.
- Savre, J., and A. M. L. Ekman (2015), Large-eddy simulation of three mixed-phase cloud events during ISDAC: Conditions for persistent heterogeneous ice formation, *J. Geophys. Res. Atmos.*, *120*, 7699–7725, doi:10.1002/2014JD023006.
- Schreier, M., H. Mannstein, V. Eyring, and H. Bovensmann (2007), Global ship track distribution and radiative forcing from 1 year of AATSR data, *Geophys. Res. Lett.*, *34*, L17814, doi:10.1029/2007GL030664.
- Seifert, A., and K. D. Beheng (2006), A two-moment cloud microphysics parameterization for mixed-phase clouds. Part 1: Model description, *Meteorol. Atmos. Phys.*, *92*, 45–66.
- Shupe, M. D., S. Y. Matrosov, and T. Uttal (2006), Arctic mixed-phase cloud properties derived from surface-based sensors at SHEBA, *J. Atmos. Sci.*, *63*, 697–711.
- Solomon, A., G. Feingold, and M. D. Shupe (2015), The role of ice nuclei recycling in the maintenance of cloud ice in Arctic mixed-phase stratocumulus, *Atmos. Chem. Phys.*, *15*, 10,631–10,643.
- Turner, D. D., S. A. Clough, J. C. Liljegren, E. E. Clothiaux, K. E. Cady-Pereira, and K. L. Gaustad (2007), Retrieving liquid water path and precipitable water vapor from Atmospheric Radiation Measurement (ARM) microwave radiometers, *IEEE Trans. Geosci. Remote Sens.*, *45*, 3680–3690.
- Twomey, S. (1977), The influence of pollution on the shortwave albedo of clouds, *J. Atmos. Sci.*, *34*, 1149–1152.
- Verlinde, J., et al. (2007), The mixed-phase Arctic cloud experiment, *Bull. Am. Meteorol. Soc.*, *88*, 205–221, doi:10.1175/BAMS-88-2-205.
- Verutbankul, V., F. J. Brechtel, R. Bahreini, N. L. Ng, M. D. Keywood, J. H. Kroll, R. C. Flagan, J. H. Seinfeld, A. Lee, and A. H. Goldstein (2006), Hygroscopicity of secondary organic aerosols formed by oxidation of cycloalkenes, monoterpenes, sesquiterpenes, and related compounds, *Atmos. Chem. Phys.*, *6*, 2367–2388.
- Wegener, A. (1911), *Thermodynamik Der Atmosphäre*, J. A. Barth, Leipzig, Germany.
- Wicker, L. J., and W. C. Skamarock (2002), Time-splitting methods for elastic models using forward time schemes, *Mon. Weather Rev.*, *130*, 2088–2097.